EPR and Ligand Field Studies of Iron Superoxide Dismutases and Iron-Substituted Manganese Superoxide Dismutases: Relationships between Electronic Structure of the Active Site and Activity

Jean Philippe Renault, Catherine Verchère-Béaur, and Irène Morgenstern-Badarau*

Laboratoire de Chimie Bioorganique et Bioinorganique, Institut de Chimie Moléculaire d'Orsay, Université Paris-Sud, 91405 Orsay, France

Fumiyuki Yamakura

Department of Chemistry, Juntendo University, Inba, Chiba, Japan

Malcolm Gerloch*

University Chemical Laboratories, Lensfield Road, Cambridge, U.K.

Received January 11, 2000

The problem of metal selectivity of iron/manganese superoxide dismutases (SODs) is addressed through the electronic structures of active sites using electron paramagnetic resonance and ligand field calculations. Studies of wild-type iron(III) SOD (FeSOD) from *Escherichia coli* and from *Methanobacterium thermoautotrophicum* and iron-substituted manganese(III) SOD (Fe(sub)MnSOD) from *E. coli* and from *Serratia marcescens* are reported. EPR spectroscopy of wild-type enzymes shows transitions within all three Kramers doublets identified by their *g* values. From the temperature dependence of the observed transitions, the zero-field splitting is found to be negative, $D = -2 \pm 0.2$ cm^{-1}. The electronic structure is typical of a distorted trigonal bipyramid, all the EPR features being reproduced by ligand field analysis. This unique and necessary electronic structure characterizes wild-type enzymes whatever their classification from the amino acid sequence into iron or manganese types, as *E. coli* FeSOD or *M. thermoautotrophicum* FeSOD. In iron-substituted manganese SODs, reduced catalytic activity is found. We describe how inhomogeneity of all reported substituted MnSODs might explain the activity decrease. EPR spectra of substituted enzymes show several overlapping components. From simulation of these spectra, one component is identified which shares the same electronic structure of the wild-type FeSODs, with the proportion depending on pH. Ligand field calculations were performed to investigate distortions of the active site geometry which induce variation of the excitation energy of the lowest quartet state. The corresponding coupling between the ground state and the excited state is found to be maximum in the geometry of the native SODs. We conjecture that such coupling should be considered in the electron-transfer process and in the contribution of the typical electronic structure of FeSOD to the activity.

Introduction

Superoxide dismutases (SODs) are metalloenzymes which catalyze the disproportionation of the superoxide anion O_2^- to dioxygen and hydrogen peroxide according to the one-electron redox cycle:

$$2O_2^- + 2H^+ \rightleftharpoons O_2 + H_2O_2$$

Interest in these proteins is strong since superoxide appears to play an important role in several diseases with cellular degenerative processes arising under oxidative stress conditions.

Three main classes of superoxide dismutases have been reported, differing in their sequence, structure, and metallic cofactors. Crystallographic structures have been published for proteins of each class with Cu-, Fe-, or Mn-containing active sites. They are reported to be able to catalyze superoxide disproportionation when associated with their native cofactor, except cambialistic SODs, which do not show such selectivity and are active with either iron or manganese cofactors.

Iron and manganese SODs (FeSOD and MnSOD), which are widely distributed in bacteria, are closely related.[1] They show high sequence and close structural homology.[2,3−7] The active

* To whom correspondence should be addressed. (I.M.-B.) Phone: 33.1.69157831. Fax: 33.1.69157281. E-mail: imorgens@icmo.u-psud.fr. (M.G.) E-mail: mg10@cus.cam.ac.uk.

(1) Smith, M. W.; Doolittle, R. F. *J. Mol. Evol.* **1992**, *34*, 175−184.
(2) Lah, M. S.; Dixon, M. M.; Pattridge, K. A.; Stallings, W. C.; Fee, J. A.; Ludwig, M. L. *Biochemistry* **1995**, *34*, 1646−1660.
(3) Stoddart, B. L.; Howell, P. L.; Ringe, D.; Petsko, G. A. *Biochemistry* **1990**, *29*, 8885−8893.
(4) Schmidt, M.; Meier, B.; Parak, F. *J. Biol. Inorg. Chem.* **1996**, *1*, 532−541.
(5) Cooper, J. B.; McIntyre, K.; Badasso, M. O.; Wood, S. P.; Zhang, Y.; Garbe, T. R.; Young, D. *J. Mol. Biol.* **1995**, *246*, 531−544.
(6) Edwards, R. A.; Baker, H. M.; Whittaker, M. M.; Whittaker, J. W.; Jameson, G. B.; Baker, E. N. *J. Biol. Inorg. Chem.* **1998**, *3*, 161−171.
(7) Borgstahl, G. O. E.; Parge, H. E.; Hickey, M. J.; Beyer, W. F., Jr.; Hallewell, R. A.; Tainer, J. A. *Cell* **1992**, *71*, 107−118.

10.1021/ic0000451 CCC: $19.00
Published on Web 05/23/2000

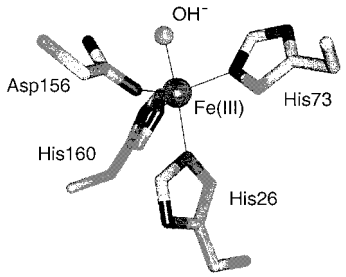

Figure 1. Active site of the iron(III) superoxide dismutase from *E. coli*. Reprinted from ref 2. Copyright 1995 American Chemical Society.

sites contain a single metal ion—either high-spin iron(III) or manganese(III)—in the native enzyme. The metal center (Figure 1) is bound by equivalent residues, two histidines and one aspartate as equatorial ligands, one axially coordinated histidine, and, most probably, a hydroxide as a fifth ligand completing a trigonal bipyramidal coordination polyhedron.[2] Several conserved noncoordinating aromatic residues which envelope the active site form a small funnel through which superoxide can reach the metal ion. However, despite many similarities, these enzymes exhibit strict metal selectivity in their activity. Except for cambialistic SODs,[8,9] manganese-substituted FeSODs (Mn(sub)FeSODs)[10,11] and iron-substituted MnSODs (Fe(sub)MnSODs)[12−14] retain little or no enzymatic activity.

The mechanism for metal-specific activity of metalloenzymes is an important point to address in the biological problem of metal recognition. The iron/manganese SOD family has been proposed as an appropriate model for this activity, but this remains to be settled.[15] Some structural variations revealed by sequence alignments[16] were analyzed from high-resolution crystallography of *Escherichia coli* FeSOD and *Thermus thermophilus* MnSOD.[2] However, these comparisons were reported as not offering any obvious clues to metal selectivity. Also, modifications of noncoordinating residues have been shown to have little or no effect on the structural properties of the active site, although some slightly reduced activity was observed. For example, mutagenesis at tyrosine position 34—which is a conserved residue in all Fe- and MnSODs—to introduce phenylalanine has been intensively studied.[17−19] *E. coli* FeSOD and MnSOD mutants exhibit specific activities 20% lower than those of wild-type enzymes.

During the last three years, some data have become available to explain, partly at least, activity changes in many metal-exchanged SODs.[13−15,18,20,21] For example, pH-dependent activity changes associated with EPR spectrum modifications were reported for Fe-substituted MnSODs from *E. coli*[18] and from *Serratia marcescens*.[13] Increasing activity was found with decreasing pH from 1% (pH 8.1) to 10% (pH 6.0) of that of the native MnSOD accompanied by changes in the iron environment as observed by EPR experiments.

Analogous high-pH inactive forms were also found in FeSOD[22] and cambialistic SOD such as *Mycobacterium smegmatis* SOD[21] but with a significantly higher interconversion pH. This pH-dependent activity change, usually interpreted[22,23] as a competitive inhibition by OH^-, was proposed as part of the mechanism of metal selectivity such that differences in the protein environment may cause the difference in the p*K* value of OH^- binding to the iron.

Very recent structural studies of Fe(sub)MnSODs from *E. coli*[24] and from *Propionibacterium shermanii*[23] clearly demonstrate that hydroxide binding modifies the Fe(III) center in these active sites and correlates with decreased dismutase activity.

Similarly, pH-dependent activity changes have been studied in Fe(sub)MnSOD mutants with phenylalanine introduced at the tyrosine 34 position.[18] Comparison with wild-type Fe(sub)-MnSOD shows that the mutant protein is more active at high pH, the maximum activity at low pH being 20% of the activity of the manganese-containing enzyme. Thus, mutagenesis of the gateway tyrosine residue was reported as relaxing the metal specificity of SODs.

Another explanation has been proposed recently.[15] The redox potential of $E°$ of the active site iron was found to be much lower for iron in the MnSOD protein than in FeSOD. To explain the corresponding inactivity of the substituted enzyme, it was suggested that proteins tend to apply $E°$ tuning appropriate for the native metal ion to whatever metal ion is bound.

To the best of our knowledge, origins of changes in either p*K* or redox potentials which have severe effects on the active site properties are not yet clear.

To address this important point and to clarify further the mechanism of metal selectivity, we have made a thorough study of the electronic structures and ligand field properties of the Fe/Mn SOD family active sites. To this end, we have focused on iron(III) enzymes—native iron(III) SODs and iron(III)-substituted manganese SODs. High-spin iron(III) is a good probe to investigate electronic properties using EPR spectroscopy and to provide ligand field data for cellular ligand field (CLF) analysis. We demonstrate, in this study, that the same unique features of the iron active site—namely, the electronic structure in the wild-type FeSOD—must be present in the Fe-substituted MnSOD to facilitate catalysis. In other words, zero-field splittings and effective g values of the $S = 5/2$ ground state obtained from EPR temperature-dependent intensities define characteristic ligand field properties appropriate for enzyme function. Ligand field calculations reproduce these electronic properties essentially perfectly. We also simulate small changes in the structural environment which might be expected to cause large effects on the electronic structure. We conjecture that one requirement for metal activity is the unique electronic structure of the wild-type FeSOD.

We describe EPR experiments for FeSODs from *E. coli* and from *Methanobacterium thermoautotrophicum*[25,26] and for Fe-

(8) Martin, M. E.; Byers, B. R.; Olson, M. J. O.; Salin, M. L.; Arceneaux, J. E. L.; Tolbert, C. *J. Biol. Chem.* **1986**, *261*, 9361−9367.
(9) Meier, B.; Barra, D.; Bossa, F.; Calabrese, L.; Rotilio, G. *J. Biol. Chem.* **1982**, *257*, 13977−13980.
(10) Yamakura, F. *J. Biochem.* **1978**, *83*, 849−857.
(11) Yamakura, F.; Suzuki, K. *J. Biochem. (Tokyo)* **1980**, *191−196*.
(12) Ose, D. E.; Fridovich, I. *Arch. Biochem. Biophys.* **1979**, *194*, 360−364.
(13) Yamakura, F.; Kobayashi, K.; Ue, H.; Konno, M. *Eur. J. Biochem.* **1995**, *227*, 700−706.
(14) Yamakura, F.; Matsumoto, T.; Kobayashi, K. In *Frontiers of reactive oxygen species in biology and medecine*; Asada, K., Yoshikawa, T., Eds.; Elsevier Science: Amsterdam, 1994; pp 115−118.
(15) Vance, C. K.; Miller, A. F. *J. Am. Chem. Soc.* **1998**, *120*, 461−467.
(16) Parker, M. W.; Blake, C. C. F. *FEBS Lett.* **1988**, *229*, 377−382.
(17) Sorkin, D. L.; Duong, D. K.; Miller, A.-F. *Biochemistry* **1997**, *36*, 8202−8208.
(18) Whittaker, M. M.; Whittaker, J. W. *Biochemistry* **1997**, *36*, 8923−8931.
(19) Guan, Y.; Hickey, M. J.; Borgstahl, G. O. E.; Hallewell, R. A.; Lepock, J. R.; O'connor, J.; Hsieh, Y.; Nick, H. S.; Silverman, D. N.; Tainer, J. A. *J. Biol. Chem.* **1998**, *37*, 4722−4730.
(20) Vance, C. K.; Miller, A. F. *Biochemistry* **1998**, *37*, 5518−5527.
(21) Yamakura, F.; Kobayashi, K.; Tagawa, S.; Morita, A.; Imai, T.; Ohmori, D.; Matsumoto, T. *Biochem. Mol. Biol. Int.* **1995**, *36*.
(22) Tierney, D. L.; Fee, J. A.; Ludwig, M. L.; Penner-Hahn, J. E. *Biochemistry* **1995**, *34*, 1661−1668.
(23) Meier, B.; Scherk, C.; Schmidt, M.; Parak, F. *Biochem. J.* **1998**, *331*, 403−407.
(24) Edwards, R. A.; Whittaker, M. M.; Whittaker, J. W.; Jameson, G. B.; Baker, E. N. *J. Am. Chem. Soc.* **1998**, *120*, 9684−9685.

substituted MnSODs from *E. coli* and from *S. marcescens*.[13] They are followed by ligand field calculations, using the CLF model, to correlate electronic properties and metal ion specific activity of the active site. A preliminary account of the work on FeSOD has been communicated previously.[27]

Experimental Section

Materials. Unless otherwise stated, chemicals were purchased from Sigma and used without purification.

Bacterial Growth, Protein Purification, and Preparation of Metal Reconstituted Proteins. FeSOD from *E. coli* was purchased from Sigma.

FeSOD from *M. thermoautotrophicum.* The plasmid containing the *M. thermoautotrophicum* SOD gene was a generous gift from Dr. M. Takao (Tohoku University). It was used to transfect the *E. coli* strain BL21 λ DE5 (pLysS). The bacteria were grown in a LB medium supplemented with 100 μg/mL ampicillin and 100 μM $Fe^{II}SO_4$ salts. Additions of glucose (up to 2%) and ampicillin were made, depending on the growth of bacteria (followed at 600 nm). All cultures were made in a 4 L homemade fermentor, saturated with dioxygen, at 37 °C. The protein was obtained as described previously,[25] except that in the ion-exchange chromotography step, a Resource Q column (Pharmacia) was used. The final gel filtration step was conducted on a Sephadex G200 100 × 1 cm column.

Fe(sub)MnSOD from *E. coli* was obtained from *E. coli* harboring the pDT1-plasmid.[28] Iron was introduced in vivo, by growing the bacteria in an M9 minimal medium depleted of metals by chromatography on Chelex resin, and enriched afterward in $Fe^{II}SO_4$ (100 μM) and ampicillin (100 μg/mL). Further additions of glucose (up to 1%) were made when the optical density reached 0.8. Iron-substituted maganese SOD was purified by ammonium sulfate precipitation between 50% and 80%. After dialysis for 5 days at pH 7.8, the extracts were chromatographed on HiTrap Q (Tris−HCl gradient, pH 7.8, 5−50 mM). The fractions containing MnSOD were pooled and chromatographed by gel filtration on a Sephadex G100 100 × 1 cm column. Sample purity was checked by denaturating and nondenaturating polyacrylamide gel electrophoresis.

Fe-substituted MnSOD from *S. marcescens* was obtained as described previously.[13]

EPR Measurements. EPR spectra were recorded with a Bruker ER-200D spectrometer operating at the X-band frequency of 9.43 GHz and provided with a helium continuous-flow cryostat (Oxford Instruments). The microwave power was 10 dB and modulation amplitude 4 G. Samples were dialyzed, concentrated by lyophilization and diluted in the appropriate buffer. All pH values were equilibrated after redissolution. Samples recorded at pH 7.8 were buffered with Tris−HCl (50 mM), and samples recorded at pH 6 were buffered with potassium acetate (50 mM). Final protein concentrations were 0.5 mM for *E. coli* FeSOD, 0.5 mM for *S. marcescens* Fe(sub)MnSOD, 1 mM for *E. coli* Fe(sub)MnSOD, and 3 mM for *M. thermoautotrophicum* FeSOD. Solutions were degassed with argon prior to use. They were mounted in standard 4 mm quartz EPR tubes with no addition of cryoprotectant. Temperature-dependent intensities of the observed transitions were collected within the temperature range 4−25 K. As the line width does not appear to broaden appreciably in the temperature range used, the EPR intensity was measured by the amplitude of specific signals. Non-power-saturation conditions were checked at the lowest temperature. Temperatures were carefully calibrated with a rhodium−nickel thermocouple sensor located in the EPR cavity at the sample position.

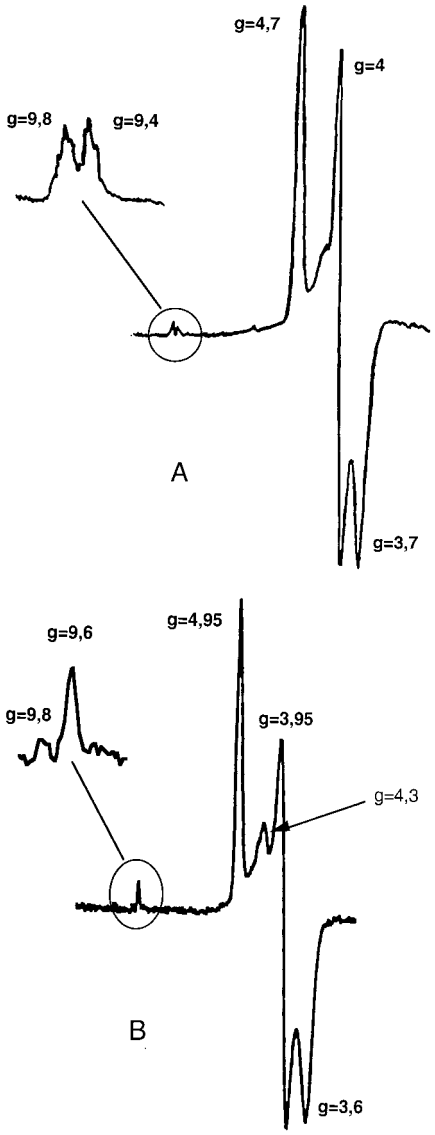

Figure 2. EPR spectra of the iron superoxide dismutase from *E. coli* (A) and from *M. thermoautotrophicum* (B), in Tris−HCl, pH 7.8. The *E. coli* spectrum was recorded at 7 K and that of the *M. thermoautotrophicum* at 15 K.

EPR Simulations. These were made using a program written by H. Wu,[29] based on the simulation procedures described by A. S. Yang and B. J. Gaffney.[30]

Ligand Field Calculations. CAMMAG and CLF model. The CAMMAG program[31] running on a Silicon Graphics Indy workstation was used for all calculations. CAMMAG uses the CLF model[32] to calculate d−d transition energies, *g* values and zero-field splittings for the d^5 metal center perturbed by Coulomb, spin−orbit coupling, and ligand field effects. The latter are locally parametrized with variables which relate directly to geometry and chemical bonding features. Calculations have been performed within bases comprising (a) all free-ion terms arising from the d^5 configuration and (b) the ground ^6S and all spin-quartet terms. EPR *g* factors and zero-field splittings reproduced within these two bases differ by less than 1%. Tabulated results relate to the complete d^5 basis.

(25) Takao, M.; Yasui, A.; Oikawa, A. *J. Biol. Chem.* **1991**, *266*, 14151−14154.
(26) Takao, M.; Oikawa, A.; Yasui, A. *Arch. Biochem. Biophys.* **1990**, *283*, 210−216.
(27) Morgenstern-Badarau, I. In *Bioinorganic Chemistry: an inorganic perspective of life*; Kessissoglou, D., Ed.; NATO ASI Series, Vol. 459; Kluwer Academic Publishers: Dordrecht, The Netherlands, 1994; Vol. 459, pp 105−113.
(28) Touati, D. *J. Bacteriol.* **1983**, *155*, 1078−1087.
(29) Wu, H. *J. Mol. Graph.* **1996**, *16*, 338−340.
(30) Yang, A.-S.; Gaffney, B. J. *Biophys. J.* **1987**, *51*, 55−68.
(31) Gerloch, M. *Magnetism and Ligand Field Analysis*; Cambridge University Press: Cambridge, U.K., 1983.
(32) Bridgeman, A. J.; Gerloch, M. *Prog. Inorg. Chem.* **1987**, *45*, 179−281.

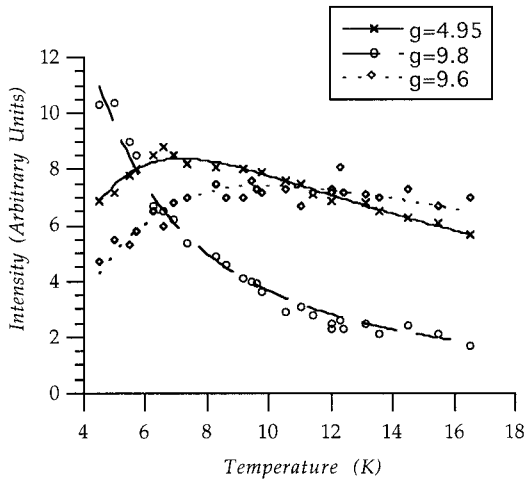

Figure 3. Temperature dependence of selected signals in the *M. thermoautotrophicum* FeSOD EPR spectrum.

Results

(1) EPR Studies of wild-type FeSODs. EPR spectra of FeSODs from *E. coli* and *M. thermoautotrophicum* are shown in Figure 2. They reveal three intense signals in the 1500 G region with effective *g* values equal to 4.7, 4.0, and 3.7 for *E. coli* (Figure 2A) and 4.95, 3.95, and 3.62 for *M. thermoautotrophicum* (Figure 2B). Two further weak signals appear at low field, with the corresponding effective *g* values of 9.8 and 9.4 for the first protein and 9.8 and 9.6 for the second. These *g* values clearly suggest that the electronic structures of the active sites are closely similar. They are consistent with those expected for high-spin iron(III) molecules with an $S = 5/2$ ground state subject to zero-field splitting which resolves the 6-fold degeneracy into three Kramers doublets, with predominant spin character 1/2, 3/2, and 5/2. Samples also display a small signal at $g_{eff} = 4.3$ which is very often observed in iron proteins and which is very likely due to nonspecifically bound iron(III).

Assignment of each doublet is made from the temperature dependencies of the resonance intensities, which are displayed for FeSOD from *M. thermoautotrophicum* in Figure 3. The intensity of the "9.8" resonance decreases with increasing temperature. The three intense signals around $g_{eff} = 4$ are characterized by a maximum intensity at 9 K (only one of them, the "4.7" signal intensity, is shown in Figure 3 since all three show the same temperature behavior). The intensity of the "9.6" signal reaches a maximum at 18 K. Therefore, the 9.8 resonance can be assigned to the ground doublet, whereas the three intense transitions arise from the intermediate doublet and the 9.6 transition arises from the second excited doublet. Similar features are observed from the EPR study of *E. coli* FeSOD (Figure S1, Supporting Information).

The rhombicity, *E*/*D*, is estimated by fitting the effective *g* values to theoretical equations published by H. Wickman[33] using the spin-Hamiltonian formalism:

$$\mathbf{H_S} = D_S(\mathbf{S_z}^2 - {}^1/_3\mathbf{S}^2) + E_S(\mathbf{S_x}^2 - \mathbf{S_y}^2) + \beta(\mathbf{S}(g_S)B) \quad (1)$$

where the spin-Hamiltonian parameters have their usual meanings. *E*/*D* values are found to be 0.23 for *E. coli* and 0.22 for *M. thermoautotrophicum*, defining significant distortions from axial symmetry. This is confirmed by the three signals belonging to the intermediate Kramers doublet, the typical isotropic resonance at "4.3" being resolved in three components when the rhombic parameter is less than $E/D = 1/3$.[33]

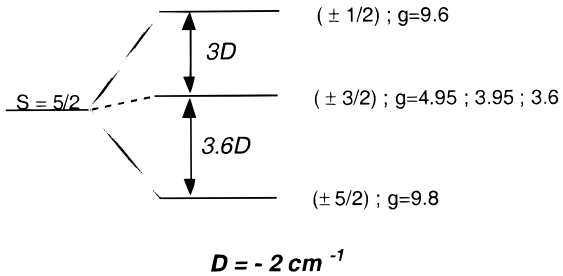

Figure 4. Electronic structure associated with the sextuplet ground state of iron(III) in *M. thermoautotrophicum* superoxide dismutase.

The consistency of observed and calculated *g* values associated with all three doublets for $E/D = 0.23$ (or 0.22), on one hand, and the assignment of the $g_{eff} = 9.8$ value to the ground doublet from the temperature dependence of intensity, on the other, provide identification of each doublet in terms of the six (S, M_s) functions. The description of the ground state is established as wave functions with predominant spin character 5/2, defining the zero-field splitting as negative.

The zero-field splitting parameter, *D*, can be estimated from the temperature dependence of the transition intensities using the Boltzmann distribution within the three Kramers levels 5/2, 3/2, and 1/2, where $\pm M_s$ represents mixed M_s functions with predominant M_s parentage. The respective intensities, *I*, are proportional to the *F* functions:

$$F_1 \approx 1/\{T(1 + \exp(-3.6D/kT) + \exp(-6.6D/kT)\}$$
$$F_2 \approx \exp(-3.6D/kT)/\{T(1 + \exp(-3.6D/kT) + \exp(-6.6D/kT)\} \quad (2)$$
$$F_3 \approx \exp(-6.6D/kT)/\{T(1 + \exp(-3.6D/kT) + \exp(-6.6\ D/kT)\}$$

where 3.6 and 6.6 D are the energies of the excited doublets relative to the ground state. The rhombic parameter *E* is included in the 3.6 and 6.6 factors obtained from the *E*/*D* value equal to 0.23.[33] The resonance intensity *I* is expressed for each isolated doublet perturbed by the Zeeman effect in first order. Each is related to the following expression:

$$I = F[g_{eff}^2 M_s^2] \quad (3)$$

We find that $D = -2 \pm 0.2$ cm^{-1} for both proteins.[34] The associated electronic structure of the ground state is shown in Figure 4.

(2) EPR Studies of Fe-Substituted MnSODs. Protein Substitution Method. Preliminary metal exchange experiments have been conducted by Fridovich on *E. coli* MnSOD to produce nonstoichiometrically substituted SODs.[12] However, this method has been successfully used by Yamakura et al. for other MnSODs, especially the Fe(sub)MnSODs from *S. marcescens* and *M. smegmatis*.[13,21]

The iron substitution problem in *E. coli* can be overcome in two ways. Miller et al. have used reducing dialysis.[15,20] We have developed an in vivo substitution similar to that of Whittaker et al.[18] This method uses the fact that, during the production of

(33) Wickman, H. H.; Klein, M. P.; Shirley, D. A. *J. Chem. Phys.* **1965**, *42*, 2113.

(34) Our results are in agreement with those found for *Azotobacter vinelandii* FeSOD (Emptage, M. H. Fed. Proc., Fed. Am. Soc. Exp. Biol. 1981, *40*, 1798).

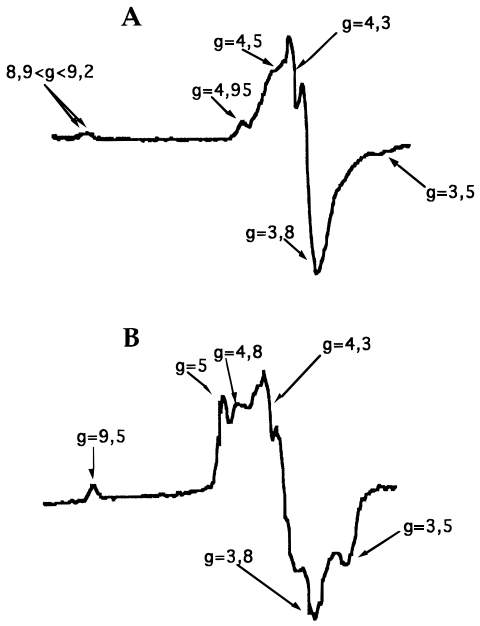

Figure 5. EPR spectra of the iron-substituted manganese SOD from *E. coli* (A) and from *S. marcescens* (B) in Tris−HCl, pH 6. Both spectra were recorded at 5 K.

MnSOD, the nature of the metal cofactor is dependent upon the metal supply. Either a depletion in manganese or an excess of iron in the medium may induce the production of Fe(sub)-MnSOD. Whittaker uses an excess of iron in the bacterial culture medium to produce Fe(sub)MnSOD, whereas we try to remove all manganese traces in our preparations beforehand. Both methods yielded samples with the same spectroscopic properties.

EPR Experiments. We measured EPR spectra at liquid helium temperatures for Fe(sub)MnSODs from *E. coli* and from *S. marcescens*. As these two SODs regain some activity at low pH, we performed EPR experiments at pH 6. Similar high-spin iron(III) spectra were recorded. They show overlapping signals from several species which are formed at this pH (Figure 5).

We have simulated the EPR spectra to identify the different components corresponding to each species. We reproduce the main typical features of the intermediate Kramers doublet around $g_{\text{eff}} = 4.3$ as shown in Figure 6 by incorporating four (for *E. coli* Fe(sub)MnSOD) or five (for *S. marcescens* Fe(sub)MnSOD) different components into the simulation (Table 1).

Component I is a spectrum similar to the spectra of the wild-type enzymes with effective g values equal to 5.0, 3.8, and 3.5 for the more intense doublet, and $E/D = 0.22$. An estimation of the zero-field splitting, D, was obtained from temperature dependent intensity studies as described above (Figure S2). We find $|D| = 3\ \text{cm}^{-1}$. Resonances at lower field are not well resolved, and therefore the sign of D is not determined. We assume that this component is the active form of iron-substituted manganese SODs, in agreement with previous work of Yamakura on *S. marcescens* SOD, who reported strong correlation between the intensity of the signals and the SOD activity.[13]

The other components correspond to more rhombic species with smaller D values compared to component I. Results obtained from simulation of the overlapping spectra are displayed in Table 1.

(3) Ligand Field Analysis. In this section, first, we report a ligand field analysis which focuses attention upon the energy separation Δ from the ground spin-sextet term to the first excited quartet terms. Second, we model that sextet−quartet excitation energy as a function of geometry, at least as far as small departures from the real geometry are concerned.

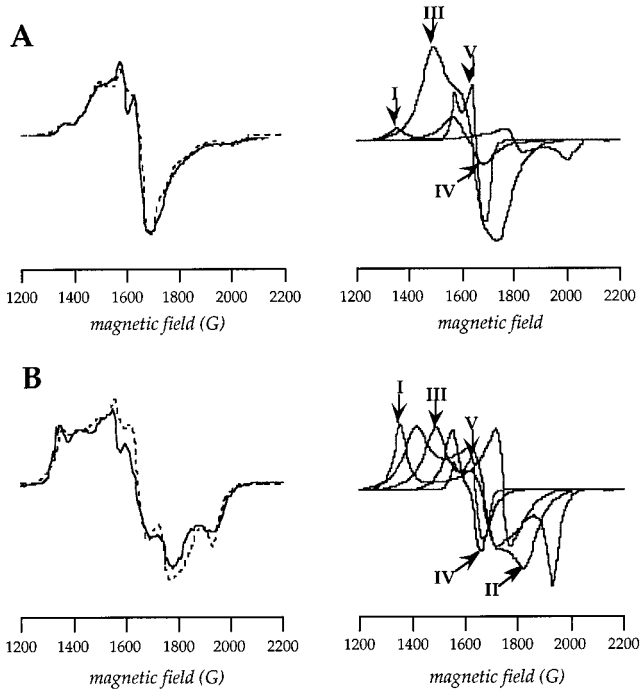

Figure 6. Overlay of experimental (solid line) and simulated (dashed line) EPR specta of the iron-substituted manganese SOD from *E. coli* (A) and from *S. marcescens* (B). Arrows indicate the positions at which EPR intensity is read. The overlapping components of the EPR spectra are detailed for each enzyme on the right. The simulation parameters for these components are listed in Table 1.

Geometry and Parametrization. Calculations relate to the *E. coli* FeSOD structure. The parameter set which is predicated upon the ligand coordinates and orientations established by the X-ray diffraction (Figure 1) recognizes four different ligation types: the two equatorial histidines (His73 and His160), N_{eq}; the equatorial carboxylate (Asp156), O_{eq}; the axial histidine (His26), N_{ax}; the axial hydroxide, O_{ax}. σ-interactions with each ligand type are parametrized with $e_\sigma(N_{eq})$, $e_\sigma(O_{eq})$, $e_\sigma(N_{ax})$, and $e_\sigma(O_{ax})$. π-interactions normal to the heterocyclic histidine planes are represented by $e_{\pi_\perp}(N_{eq})$ and $e_{\pi_\perp}(N_{ax})$. π-interactions parallel to these ligand planes are presumed to be zero. We also recognize interaction with the p_π lone pair on carboxylate (and hydroxide) with $e_{\pi_\perp}$. We have taken no account of in-plane π-type interactions with these two ligands.

Holohedral symmetry within the pure d electron basis reduces the degree of parametrization presented so far. Thus, perturbations on diametrically opposite sides of the metal are strictly inseparable. One cannot distinguish $e_\lambda(O_{ax})$ from $e_\lambda(N_{ax})$; $\lambda = \sigma$, π_x, and π_y. Accordingly, the total axial σ perturbation is represented by $e_\sigma(ax) = e_\sigma(O_{ax}) + e_\sigma(N_{ax})$. Similarly, $e_{\pi_x}(ax) = e_{\pi_x}(O_{ax}) + e_{\pi_x}(N_{ax})$ and $e_{\pi_y}(ax) = e_{\pi_y}(O_{ax}) + e_{\pi_y}(N_{ax})$. However, the planes of the axial histidine and the hydrogen-bonded carboxylate−hydroxide moiety are nearly parallel to one another. Therefore, all π-interactions of the metal with the axial ligands can be approximated by $e_{\pi_\perp}(ax)$, $e_{\pi_\perp}(N_{ax})$ referring to a π-interaction that is nearly parallel with that represented by $e_{\pi_\perp}(O_{ax})$, and $e_{\pi_\parallel}(ax) = 0$.

We have fixed a common e_π/e_σ ratio for equatorial and axial ligations to reduce the parameter set to $e_\sigma(N_{eq})$, $e_\sigma(O_{eq})$, $e_\sigma(ax)$, and $e_{\pi_\perp}/e_\sigma$. To these CLF variables must be added the Racah B parameter and ζ, the one-electron, spin−orbit coupling coefficient. Parameter ranges considered in the analysis are shown in Table 2.

Reproduction of FeSOD EPR Data. We have sought to reproduce the EPR data reported above: the effective g values

Table 1. Summary of EPR Data for Iron-substituted Manganese SODs

origin	component	major *g* values	E/D[a]	D (cm^{-1})[b]	line width (G)	proportion (%)
E. coli	I	4.95, 3.85, 3.5	0.22	**3**	15	22
	III	4.8	0.28 (δ 0.1)	*0.6*	30	65
	IV	4.45	0.31 (δ 0.1)	*0.2*	30	7
	V	4.3, 4.15, 4	0.33	*0.2*	7	6
S. Marcescens	I	4.95, 3.85, 3.5	0.22	**3**	15	34
	II	4.5	0.25 (δ 0.1)	*0.6*	30	39
	III	4.8	0.28 (δ 0.1)	*0.3*	30	20
	IV	4.45	0.31 (δ 0.1)	*0.2*	30	5
	V	4.3, 4.15, 4	0.33	*0.2*	7	2

[a] The simulation introduces a Gaussian repartition of E/D values defined by its standard deviation δ. [b] Results in bold arise from temperature dependence studies, results in italics from simulation of overlapping spectra.

Table 2. Cellular Ligand Field Parameter Ranges for the FeSOD Active Site

e_σ(Oeq), cm^{-1}	4000−13000	$e_{\pi\perp}/e_\sigma$	0−0.5
e_σ(ax), cm^{-1}	6000−15000	B, cm^{-1}	500−1000
$e_\sigma(O_{eq})/e_\sigma(N_{eq})$	1.5−0.6	ζ, cm^{-1}	250−500

Table 3. Some Parameter (cm^{-1}) Sets Fitting Both *g* and *D* Values[a]

$e_\sigma(O_{eq})$	e_σ(ax)	B	ζ	Δ	
8250	10250	600	350	5500	set 1
8500	7750	600	450	7300	set 2
8750	12500	900	350	5900	set 3
7250	12000	600	300	4500	set 4
7750	9500	500	350	5400	set 5

[a] Δ is equal to the energy gap between the lowest quartet state and the sextet ground state.

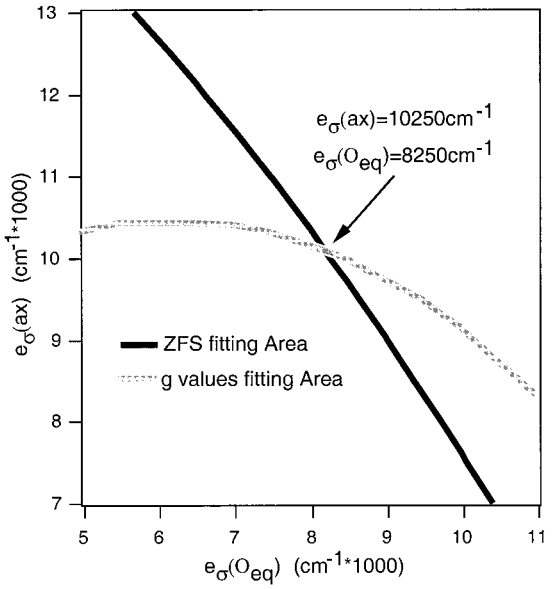

Figure 7. Determination of the e_σ parameters fitting both *g* and *D* values (B = 600 cm^{-1}, ζ = 350 cm^{-1}, $e_\sigma(O_{eq})/e_\sigma(N_{eq})$ = 1.5, $e_{\pi\perp}/e_\sigma$ = 0.1).

for each Kramers doublet and the excitation energies for the second and third Kramers doublets (Figure 4).

All EPR data were reproduced well but with parameter values correlated within wide ranges (Table 3). Typical of them is the intersection of *g* and zero-field splitting fitting areas, shown for a specific parameter set in Figure 7, which establishes reasonably unique $e_\sigma(O_{eq})$ and e_σ(ax) values for a given choice of B and ζ parameters and of $e_\sigma(O_{eq})/e_\sigma(N_{eq})$ ratio.

The dependencies of *good* fits upon B and ζ are shown in Figure 8; appropriate but different values of $e_\sigma(O_{eq})$ and $e_\sigma(N_{ax})$ are associated with different B and ζ values. The energy separation $\Delta = E$(lowest quartet state) − E(sextet ground state)

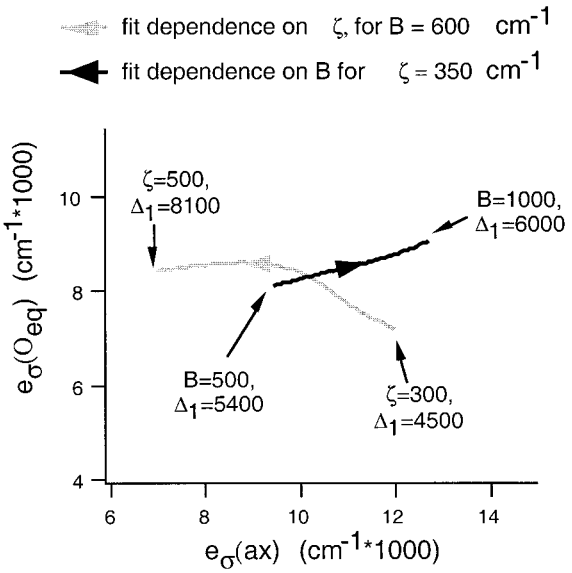

Figure 8. Dependence of the e_σ parameters fitting both *g* and *D* values on B and ζ ($e_\sigma(O_{eq})/e_\sigma(N_{eq})$ = 1.5, $e_{\pi\perp}/e_\sigma$ = 0.1).

Table 4. Quality of the Fit for Parameter Set 1[a]

	Kramers doublet ±5/2	Kramers doublet ±3/2	Kramers doublet ±1/2
exptl *g* values	9.8	4.7, 4.0, 3.7	9.4
exptl energies		7.2	13.2
calcd *g* values	9.81	4.75, 4.1, 3.75	9.4
calcd energy		7.7	13.7

[a] B = 600 cm^{-1}, ζ = 350 cm^{-1}, $e_{\pi\perp}/e_\sigma$ = 0.1, $e_\sigma(O_{eq})$ = 8250 cm^{-1}, $e_\sigma(N_{eq})$ = 5500 cm^{-1}, and e_σ(ax) = 10250 cm^{-1}. The energies of the excited Kramers doublets are expressed in cm^{-1}.

varies with these correlations, as shown in Table 3. Unsurprisingly, good fits to zero-field splittings require larger D values to be associated with larger ζ values. Overall, the correlations illustrated in Figure 8 and Table 3 are such that, in any case, within the large parameter ranges explored, the sense of the calculated zero-field splitting (the sign of D) is the same. Table 4 illustrates the quality of the fit for a typical successful parameter set.

For a given choice of B and ζ values, equally good reproduction of the EPR data was found for $e_\sigma(O_{eq})/e_\sigma(N_{eq})$ lying in the range 1.5−0.6, corresponding to the ligand field strength of carboxylate being stronger or weaker than that of the equatorial histidines.

Similar calculations have been performed for $e_{\pi\perp}/e_\sigma$ ratios in the range 0−0.5, the $e_\sigma(O_{eq})/e_\sigma(N_{eq})$ ratio being fixed to 1.5 by comparison with that reported for a histidine chromium compound.[35] The quality of these fits was much more sensitive to the ratio $e_{\pi\perp}/e_\sigma$, and no satisfactory fits were obtained outside

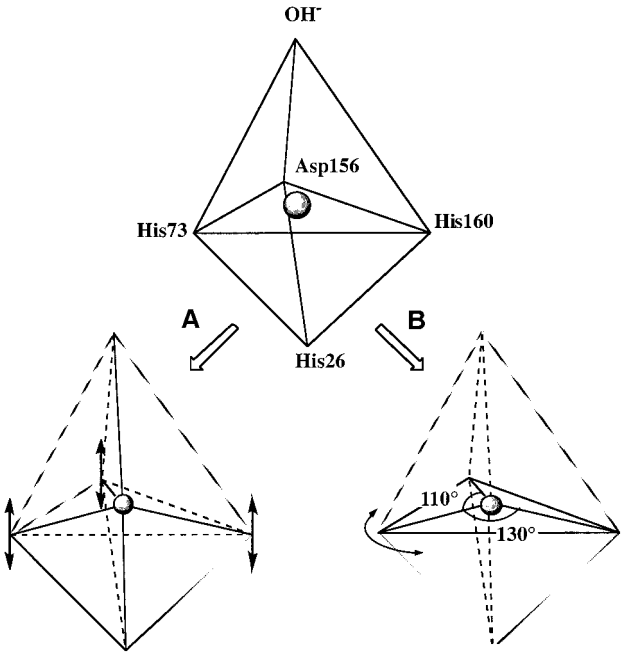

Figure 9. Notional geometric variations from the observed structure of the active site: (A) axial displacement of the iron along the 3-fold axis; (B) angular distortions within the equatorial plane.

the range 0.1−0.4. Within this range, the best fits were obtained for a $e_{\pi\perp}/e_\sigma$ ratio between 0.25 and 0.1. However, a ratio of 0.25 gives a positive D value, whereas a ratio of 0.1 gives fits with the correct negative zero-field splitting, i.e., ±5/2 being the lowest.

Holohedral symmetry denies direct, separate determination of e_σ parameters for the axial histidine and hydroxyl ligands. Estimates may be made, however, in that e_σ parameters tend to be related to the metal−ligand distance:[36−38]

$$e_\sigma(\mathrm{NHis}) \propto (d_{\mathrm{Fe-His}})^{-5}; \quad e_\sigma(\mathrm{ax}) = e_\sigma(\mathrm{N_{ax}}) + e_\sigma(\mathrm{O_{ax}}) \quad (4)$$

Using parameter set 1 for axial histidine and relations 4, we find $e_\sigma(\mathrm{His26}) = 4400\ \mathrm{cm^{-1}}$ and $e_\sigma(\mathrm{OH^-}) = 5800\ \mathrm{cm^{-1}}$ from $d_{\mathrm{Fe-His160}} = 2.05$ Å and $d_{\mathrm{Fe-His26}} = 2.15$ Å.

Altogether, therefore, we conclude that excellent reproduction of all experimental EPR data is possible using parameter values that accord well with the broadly based experience of ligand field analysis.

Geometry Variations. In this section, we report explorations of the ligand field as a function of small variations in geometry from that observed in the crystalline phase by X-ray diffraction.

The first geometry variation (Figure 9A) involves displacement of the metal atom by up to 0.3 Å along the pseudo-3-fold axis of the trigonal bipyramid. The metal displacement is accompanied by variation of the angles between axial and equatorial ligands. Because of the holohedral relationship between the axial ligands, this may be seen as a distortion toward tetrahedral geometry. We focus our attention upon Δ, the first sextet−quartet excitation energy, as g values are only weakly sensitive to this distortion. Similar results have been obtained for several choices of "good fit" parameters. They are all

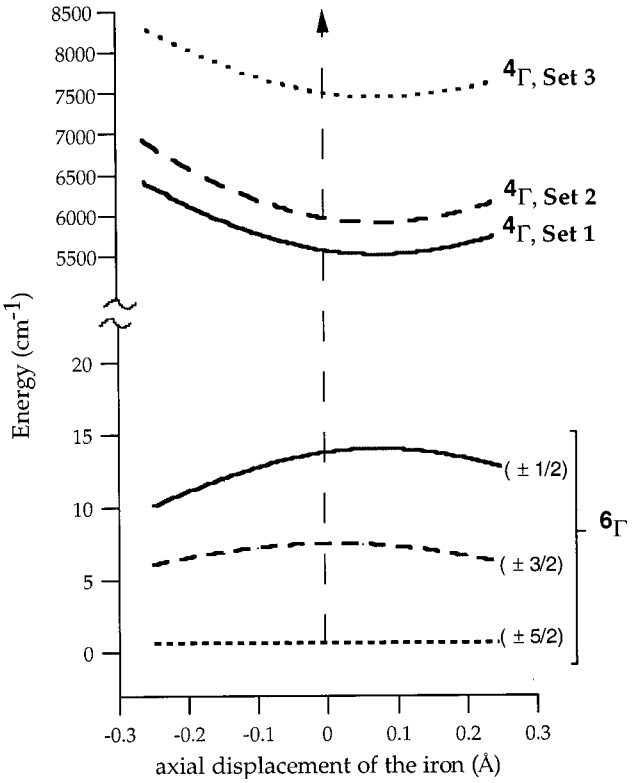

Figure 10. Variations of the zero-field splitting and of the first quadruplet term energies with axial distortion. All energies are defined with respect to the ground Kramers doublet of the sextuplet term ($e_\sigma(\mathrm{O_{eq}}) = 8250\ \mathrm{cm^{-1}}$, $e_\sigma(\mathrm{ax}) = 10\,250\ \mathrm{cm^{-1}}$, $B = 600\ \mathrm{cm^{-1}}$, $\zeta = 350\ \mathrm{cm^{-1}}$, $e_\sigma(\mathrm{O_{eq}})/e_\sigma(\mathrm{N_{eq}}) = 1.5$, $e_{\pi\perp}/e_\sigma = 0.1$).

characterized by Δ being a minimum near the observed "true" geometry, as sketched in Figure 10. The absolute magnitudes of Δ values corresponding to the displacement of the metal atom along the "trigonal" axis vary with the parameter set, of course. However, all curves display a minimum when the metal atom is coplanar with the equatorial ligand donor atoms.

We have also studied (Figure 9B) an alternative distortion of changing bond angles in the equatorial plane. The angles $\mathrm{O_{eq}-Fe-N_{eq}}$ were varied by ±20° from that observed ($\mathrm{O_{Asp156}-Fe-N_{His73}} = 110°$) by X-ray diffraction. The same parameter set 1 was used in the calculations illustrated in Figure 10, although similar results were obtained for all parameter sets. Curves in Figure 11 reveal a maximum value of Δ when the angle is nearly equal to the observed crystallographic value.

Discussion

Commonality of the Electronic Structures of *E. coli* and *M. thermoautotrophicum* Wild-Type Iron Superoxide Dismutases. EPR spectroscopy provides a revealing probe of iron(III) active sites. Experiments at liquid helium temperature are needed to observe low-field resonances, which are the only ones to determine the sign of the zero-field splitting. EPR spectra are very closely similar for both enzymes, showing resonances within each Kramers doublet. Effective g values are found to be only slightly different, and the rhombic parameters are 0.22 and 0.23. Negative zero-field splitting is found for each active site, its value being $D = -2.0 \pm 0.2\ \mathrm{cm^{-1}}$. Thus, these active sites have an essentially common electronic structure. Although no crystallographic structure is available for *M. thermoautotrophicum* FeSOD, we may be confident, from these EPR studies, that the two proteins share very similar electronic

(35) Lee, K.-W.; Eom, K.-I.; Park, S.-J. *Inorg. Chim. Acta* **1997**, *254*, 131−136.
(36) Stratemeier, H.; Hitchman, M. A.; Comba, P.; Bernhardt, P. V.; Riley, M. J. *Inorg. Chem.* **1991**, *30*, 4088−4093.
(37) Bernhardt, P. V.; Comba, P. *Inorg. Chem.* **1993**, *32*, 2798.
(38) Burton, V. J.; Deeth, R. J.; Kemp, C. M.; Gilbert, P. J. *J. Am. Chem. Soc.* **1995**, *117*, 8407−8415.

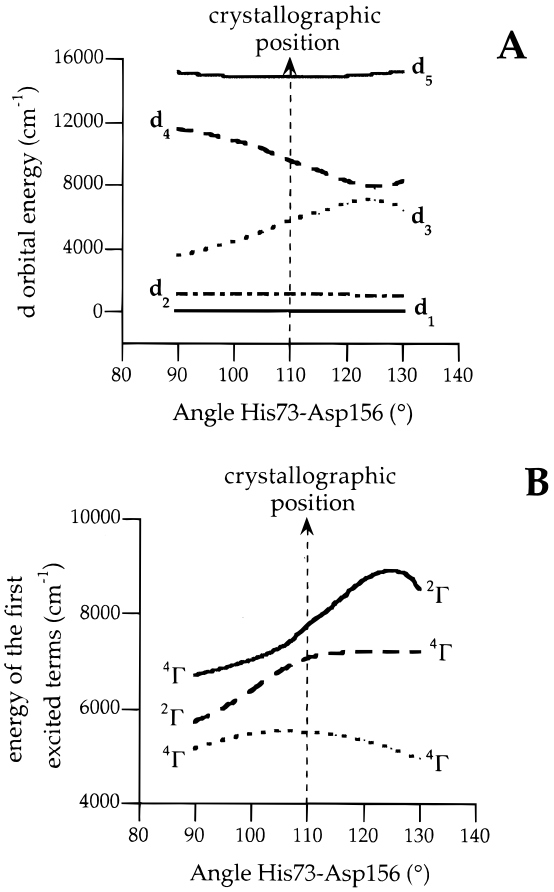

Figure 11. Variations of the d orbital energies (A) and of the first three excited term energies (B) with angular distortion. The d orbital energies are defined with respect to the lowest d orbital. For the excited terms, all energies are defined with respect to the ground Kramers doublet of the sextuplet term ($e_\sigma(O_{eq}) = 8250$ cm^{-1}, $e_\sigma(ax) = 10\,250$ cm^{-1}, $B = 600$ cm^{-1}, $\zeta = 350$ cm^{-1}, $e_\sigma(O_{eq})/e_\sigma(N_{eq}) = 1.5$, $e_{\pi\perp}/e_\sigma = 0.1$).

properties and metal environments, at least within the first coordination sphere.

It is worth pointing out that *M. thermoautotrophicum* FeSOD is assigned to the MnSOD class according to its sequence.[1,16,25] In confirmation of this, we have observed a conformational change from NMR studies on the reduced form which is similar to that reported for *E. coli* MnSOD.[39]

Thus, the structural changes in the second coordination sphere which are usually used to distinguish the MnSOD class from the FeSOD class induce minimal effects on the metal selectivity and insignificant change in the electronic structure.

Notwithstanding these classification differences, the present EPR data clearly identify a commonality in the electronic structure of the active site in the *E. coli* and *M. thermoautotrophicum* FeSODs. That electronic structure is evidenced by a negative zero-field splitting with magnitude $D = -2$ cm^{-1}, together with a rhombicity, E/D, of 0.22, and this is associated with a superoxide dismutase activity, independently of the structural details.

Comparison of Wild-Type FeSODs and Fe(sub)MnSODs EPR Properties. Several metal-exchanged SODs have been reported in the literature. Yamakura has studied iron substitution in *E. coli* and *S. marcesens* manganese SODs. EPR spectral changes were recorded as functions of pH and correlated with activity measurements.[13,14] We have performed simulations of EPR spectra from both iron-substituted enzymes, at low pH.

From several overlapping signals, we have been able to recognize four characteristic main components from our simulations. These components are also present in the EPR spectrum of *M. smegmatis* FeMnSOD, a cambialistic enzyme, at its activity pH.[21]

Yamakura found increasing activity in the Fe(sub)MnSODs to be associated with decreasing pH and increasing intensity of what is here identified as component I. The present EPR work shows that this component is characterized by the same EPR properties as in the wild-type iron SODs. This result strongly suggests that activity is correlated with electronic structure and is a function of the concentration of the species with the typical FeSOD electronic structure.

All reported examples of metal-exchanged SODs are found as inhomogeneous proteins, with the same species in various proportions. Comparisons of the activities of substituted enzymes with natural enzymes must be made with this in mind. The origin of heterogeneity is not yet clearly understood, and the control of the equilibrium between the different components is a matter to be addressed to solve the problem of metal selectivity.

We conclude, therefore, that the inhibition of enzyme activity on replacing Mn by Fe in MnSODs is not so much due to the metal substitution per se, but rather to a diminished proportion of the typical active site of wild-type FeSODs, a proportion that depends critically upon pH. While maximal activity for the native FeSOD is found at pH 7, maximal (but lower) activity for the native Fe(sub)Mn occurs at significantly lower pH.

Ligand Field Analysis of FeSOD. The CLF model recognizes details of the first coordination shell of the d center. Bond lengths are requested within the energy parameters. Angular dispositions of the ligand donor atoms, together with the orientations of the ligands about each metal−donor atom vector, are taken from the X-ray crystallographic data for the *E. coli* FeSOD. As both amino acid sequences and EPR spectra indicate strong similarity of the active site coordination in both FeSODs, our ligand field analysis is expected to be equally applicable to both. Two aspects of the CLF analysis should be emphasized: (a) all EPR data are reproducible quantitatively, and (b) the parameter values affording a good fit, reproducing the EPR data within experimental errors, are unexceptional, being in line with histidine data on model compounds, especially the ratios e_σ(His)/e_σ(OH$^-$) and $e_{\pi\perp}/e_\sigma$ as obtained from studies of Cr−histidine and hydroxy complexes.[35,40] A particular aspect of the second point is that the quite "normal" values for the e_π parameter are reasonably sensitively established by the fitting process; expressed in reverse, details of the EPR spectra require $e_{\pi\perp}/e_\sigma$ values on the order of 0.1.

We emphasize that all electronic energy splittings discussed in this paper are derived either from the theoretical CLF analysis of the experimental data or from modeling of notionally distorted iron centers.

Geometry and Electronic Structure. As a quite separate exercise, we have investigated the variation of the d electron structure as a function of geometric variations from the observed structure. Our focus in these studies has been the magnitude of Δ, the energy separation between the lowest spin-quartet and the ground spin-sextet states. Our reason for this particular interest is that one might reasonably suppose the electronic change from the sextet ground term of Fe(III) to a spin-quintet ground term of Fe(II) within the process

(39) Renault, J. P.; Morgenstern-Badarau, I.; Piccioli, M. *Inorg Chem.* **1999**, *38*, 614.

(40) Lee, K.-W.; Hoggard, P. E. *Inorg. Chem.* **1991**, *30*, 264−270.

$$Fe(III) + O_2^- \rightleftharpoons Fe(II) + O_2$$

to be mediated by the spin-quartet excited state of Fe(III). The coupling of the quartet and sextet states might lower the electronic reorganization energy of the reduction of the Fe(III)-SOD to Fe(II)SOD as illustrated in Figure 12. If this is so, we expect this reduction to be kinetically facilitated inversely in proportion to the sextet−quartet energy gap, Δ.

We have considered two geometry variations. The first relates to the location of the Fe atom with respect to the equatorial ligation (Figure 9A). Whether such variations take the form of a displacement of the central atom toward one of the apical ligands or of an angular movement of all equatorial ligands away from the ideal trigonal bipyramidal plane, the CLF modeling is adequately accomplished by displacement of the metal along the pseudo-3-fold axis of the active site. Calculations have been performed for each of the typical optimal parameter sets of Table 3. The consequent dependencies of Δ upon the metal position are shown in Figure 10. Those for parameter sets 4 and 5 essentially coincide with those for set 1. They are all characterized by a minimum value of Δ when the metal atom lies close to the crystallographic location. Such a conclusion would be anticipated for similar metal displacements within a perfect trigonal bipyramid. We note, therefore, that the native FeSOD given geometry already optimizes any putative sextet−quartet mixing within the subsequent electron transfer. The second geometry variation concerns the location of the ligands within the equatorial plane. The experimentally observed angular dispositions of these ligands are shown in Figure 9B. We note how the wide angle $N_{His73}-Fe-N_{His160}$ seemingly offers an obvious site for addition of an incoming superoxide molecule if one supposes that the first enzymatic process involves an increase in the metal coordination number from five to six, electron transfer from the superoxide to the metal, loss of dioxygen, and recovery of five coordination of the now-reduced metal atom. Indeed, an important feature of the whole enzyme will be the frustration of the iron(III)s proclivity to form a six-coordinate entity, so that a "spring-loaded" center is ideally established and ready to expand its coordination shell.[41,42]

Our contribution in this scenario is to monitor the response of Δ to an angular displacement of N_{his73} as might be the first stage of accepting an incoming superoxide ion. Results based upon parameter set 1 are shown in Figure 11. Pure orbital energies are plotted in Figure 11A (equivalent to a d^1 calculation without spin−orbit coupling), while some state energies are shown in Figure 11B. Although we wish to focus on the lowest spin-quartet in Figure 11B, we first need to explain the sense of its energy variation, that is, a maximum near the ideal trigonal bipyramid rather than a minimum. The orbitals labeled d_1, (d_2, d_3), and (d_4, d_5) in Figure 11A correspond to d_{z^2}, (d_{xy}, $d_{x^2-y^2}$), and (d_{xz}, d_{yz}) in a perfect trigonal bipyramid. The fact that d_3 and d_4 achieve near degeneracy at ca. 125° rather than 120° in that diagram reflects the nonideality of the active site geometry adopted in these calculations. The crystallographically determined angles indicated in Figure 9B show how the observed geometry is already distorted from the ideal trigonal bipyramid along the proposed reaction path. The curvature of the lowest spin-quartet in Figure 11B derives from two influences: (a) its character involves the pairing of an electron from the d_1 orbital as well as from the highest-lying d_5 and (b) the effects of spin−orbit coupling (which is included in Figure 11B), on the left-hand side of the diagram in particular, are due to the close approach of the spin-doublet to both the first and second spin-quartets. The large amount of doublet−quartet scrambling near the distortion angle 90° also serves to depress the lowest quartet.

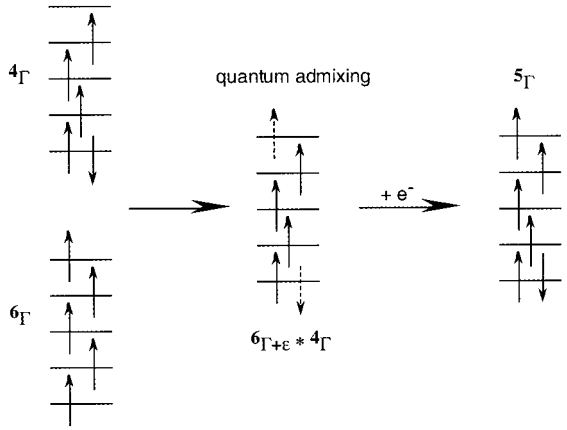

Figure 12. Configuration associated with the iron(III) quartet and sextet states, and with the iron(II) quintet state. Minimization of the electronic reorganization upon reduction is mediated by coupling of the two iron(III) states $^4\Gamma$ and $^6\Gamma$ through quantum admixing.

The significance of the curvature of this quartet is that an already reasonably proximate level would be brought even closer to the ground sextet during the course of ligand displacement, leading toward a six-coordinate, pseudooctahedral moiety. It thus seems likely that the achievement of an increased coordination number on addition of a superoxide may simultaneously even more facilitate the electron-transfer process proper.

Concluding Remarks

We have addressed the problem of SOD activity correlated to metal selectivity in iron superoxide dismutases through the electronic structures of active sites. We have found that a unique and necessary electronic structure characterizes already known wild-type iron enzymes whatever their classification from the amino acid sequence into iron or manganese types. This structure is typical of a distorted trigonal bipyramid within the first coordination shell which is common to all SOD structures and is identified by common ligand field properties.

Replacing manganese by iron in manganese SODs reduces the enzymatic activity. An understanding of this reduction in activity has long been sought. We describe how inhomogeneity of all reported substituted MnSODs might explain the activity decrease. The EPR work described here focuses attention upon a component of the substituted SODs which shares the electronic structure of the wild-type enzymes. The proportion of that component in the substituted enzymes has been shown to depend continuously upon pH.[13]

The EPR of FeSODs is here carefully characterized by the *g* values of all three Kramers doublets arising from the ground spin-sextet state as well as their energies expressed in terms of *D* and *E* parameters of zero-field splitting. All these features have been quantitatively reproduced by ligand field analysis with unexceptional parameter values.

Investigation of notional distortions of the active site geometry have centered upon the excitation energy of the lowest spin-quartet state. We discuss this quantity to present a conjecture of how coupling of the ground spin-sextet and excited spin-quartet states might lower the electronic reorganization barrier for electron transfer within the redox catalysis.[43]

(41) Williams, R. J. P. *Eur. J. Biochem.* **1995**, *234*, 363−381.
(42) Whittaker, J. W.; Whittaker, M. M. *J. Am. Chem. Soc.* **1991**, *113*, 5528−5540.
(43) Newton, M. D. *Chem. Rev.* **1991**, *91*, 767−792.

Acknowledgment. We acknowledge the very helpful comments of the reviewers. We are indebted to J. A. Fee for his generosity in providing us with the gene for MnSOD in the plasmid pDT1-5. We thank M. Takao, A. Yasui, and A. Oikawa for their generous gift of the plasmid harboring the *M. thermoautotrophicum* gene. G. Blondin is acknowledged for her help with the EPR measurements.

Supporting Information Available: Temperature dependence of selected signals in the *E. coli* FeSOD EPR spectrum (Figure S1) and temperature dependence of component I of the EPR spectra of the iron-substituted manganese SOD from *E. coli* and *S. marcescens* (Figure S2). This material is available free of charge via the Internet at http://pubs.acs.org.

IC0000451